 doi:10.20944/preprints201809.0142.v2

Article

Optimization of radiators, underfloor and ceiling heater towards the definition of a reference ideal heater for energy efficient buildings

Andrea Ferrantelli [1,*], Karl-Villem Võsa [1] and Jarek Kurnitski [1,2]

[1] Tallinn University of Technology, Department of Civil Engineering and Architecture, Ehitajate tee 5, 19086 Tallinn, Estonia; andrea.ferrantelli@taltech.ee (A.F.); Karl-Villem.Vosa@taltech.ee (K-V.V.)

[2] Aalto University, Department of Civil Engineering, P.O.Box 12100, 00076 Aalto, Finland; jarek.kurnitski@taltech.ee

* Correspondence: andrea.ferrantelli@taltech.ee; Tel.: +358-404168635

Abstract: Heat emitters constitute the primary devices used in space heating and cover a fundamental role in the energy efficient use of buildings. In the search for an optimized design, heating devices should be compared with a benchmark emitter with maximum heat emission efficiency. However, such an ideal heater still needs to be defined. In this paper we perform an analysis of heat transfer in a European reference room, considering room side effects of thermal radiation and computing the induced operative temperature both analytically and numerically. By means of functional optimization, we analyse trends such as the variation of operative temperature with radiator panel dimensions, finding optimal configurations. In order to make our definitions as general as possible, we address panel radiators, convectors, underfloor (UFH) and ceiling heater. We obtain analytical formulas for the operative temperature induced by panel radiators and identify the 10-type as our ideal radiator, while the UFH provides the best performance overall. Regarding specifically UFH and ceiling heaters, we find optimal sizes that identify the according ideal emitters. The analytical method and quantitative results reported in this paper can be generalized and adopted in most studies concerning the efficiency of different heat emitter types in building enclosures.

Keywords: radiator efficiency; energy; operative temperature; analytical model; computer simulations

1. Introduction

The energy performance of heat emitters is a key factor in the energy demand of the building sector, which is primarily determined by space heating [1–3]. Such devices can be of very different type (panel radiators, convectors, ceiling and underfloor heating...), each determining the energy demand in a specific way [4–8]. For these reasons, several studies have investigated the emitters' performance on both the experimental and theoretical viewpoint [9–11], focusing especially on the design, specific type and room placement of panel radiators (e.g. close to a window or slightly detached from a wall) [4,12–18]. For instance, measurements have shown a better performance of low temperature panel radiators [19], and a sensibly different outcome for serial and parallel connected radiators [9].

Despite such recent advances, this kind of investigation seems to be very involved, for a variety of reasons. Contrasting results also exist: an experimental investigation of a convector, a radiant and a baseboard heater showed a lower energy consumption by the convector [7], in contrast with the classic work by Olesen et al. [4], written in the early 80s. While it was concluded in [7] that the cause was probably the improved flow outlet design of the newer convector, an older study already considering this improvement [13] agreed instead with [4].

Another crucial problem is the lack of a staple or ideal emitter, to use as a reference device with maximum efficiency. For air temperature control, an ideal heater is generally described by a dimensionless point (Figure 1). Heat is transferred via convection to the thermal node of indoor air, and via radiation to the surrounding surfaces. A higher convective transfer fraction induces lower

Preprints (www.preprints.org) | NOT PEER-REVIEWED | Posted: 6 November 2018 doi:10.20944/preprints201809.0142.v2

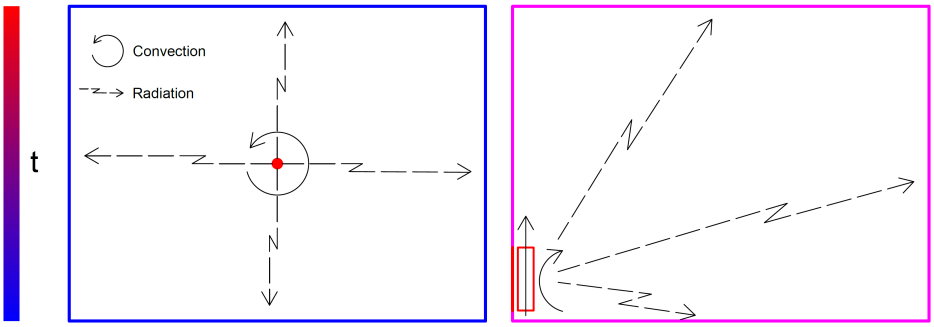

Figure 1. Ideal point heater (left) and real heat emitter (right).

surface temperatures on the surrounding surfaces with minimal heat loss, as in Fig.1. To reach the desired air temperature set-point t_{air}, an emitter with convective fraction of 1 (pure convection) thus requires the lowest possible heat output. In this sense, it represents an "ideal" heater.

Nevertheless, since heating consumption is nowadays assessed in function of thermal comfort, the so-called operative temperature (op.t.) t_{op} is being increasingly used [9,13,18,20]. This is defined as the uniform temperature of an enclosure in which an occupant would exchange the same amount of heat by radiation and convection as in the existing non-uniform environment [21]. By definition, t_{op} is thus inversely proportional to the surrounding surfaces' temperature. In this respect, the "ideal" device described above should now exhibit a lower performance, as it heats the surrounding surfaces only minimally. As we will illustrate, preliminary simulations with the software IDA ICE [22] confirm indeed that a number of real emitter configurations can outperform the point heater (or convector).

In other words, defining an ideal benchmark heater for operative temperature control is non-trivial, and needs to be addressed for better comparison between different heat emitter systems. To this aim, we consider an average-sized enclosure provided by the CEN technical committee TC130 working group WG13, with a user sitting in the middle (Figure 2). We investigate how the operative temperature changes with the typology and size of emitter, and whether there exist optimal configurations corresponding to the highest t_{op}. We address panel radiators (10- and 21-type), underfloor (UFH) square, UFH strip and ceiling heater. A 10-type radiator has only one panel and no convector fins, while the 21-type has two panels with one set of fins in between. They are illustrated in Fig.3.

In theory, any size of emitter in any configuration could be used to offset the heat loss through the external wall, with decreasingly smaller emitters requiring increasingly higher surface temperatures (naturally, supply water temperature has to rise to allow for this). However, practical reasons limit these temperatures greatly. For example, living room floor surfaces are limited to 27/29 °C in case of UFH, with higher temperatures causing thermal discomfort [23]. Large surface temperature differences in opposing directions can also cause local discomfort via a phenomena called radiant temperature asymmetry [21]. In addition, low temperature supply water can be generated with a higher thermal efficiency with ground and air source heat pumps. Higher supply water temperatures would also yield higher embedded losses. For these reasons, supply water temperature limits are imposed on the emitter systems.

By numerically computing the steady-state heat transfer in the enclosure with IDA ICE, we obtain surface temperatures for all the walls, for each specific configuration; these values are then used as boundary conditions for an analytical calculation that follows the ISO Standard [21]. The analytical calculation is necessary for two main reasons: first, as we explain in the text, IDA ICE calculates the view factors, and accordingly the mean radiant and operative temperatures, in a very specific way that

Preprints (www.preprints.org) | NOT PEER-REVIEWED | Posted: 6 November 2018 doi:10.20944/preprints201809.0142.v2

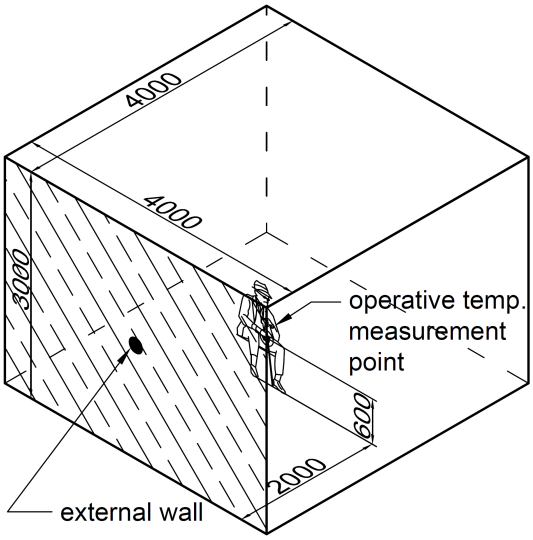

Figure 2. Room setup.

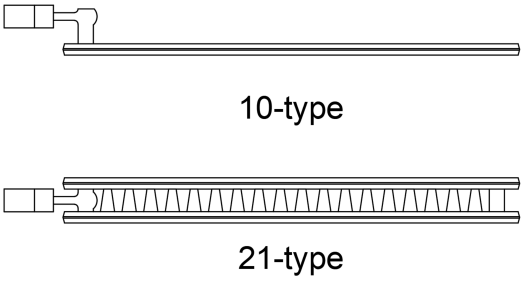

Figure 3. 10-type and 21-type panel radiators.

is different from the ISO procedure[1]. As we are aiming to contribute to the heat emission code EN 15316-2-1:200, it is advisable to use a standard procedure.

Secondly, and more importantly, we are able to extrapolate and generalize our results to *any* 10- or 21-type emitter with size included in the studied range. This is accomplished with a simple interpolation method which was introduced in [24] when assessing domestic hot water consumption.

For the case of panel radiators, keeping the heat output constant we determine analytical t_{op} curves for both the panel radiators in function of their size. This allows to rigorously highlight several features of panel radiators, such as the existence of an optimal width range for the operative temperature and a qualitative difference in t_{op} variations for the 10- and 21-type. Finally, we find that the 10-type provides the best performance and can be regarded as the "ideal" radiator.

The UFH and ceiling heater show a similar behaviour, with operative temperatures approaching, and often exceeding, the air temperature. Analytical and numerical calculations have an excellent agreement and show a maximum t_{op} for sizes smaller than the whole width of the room. The analytical solution allows to find their location precisely, up to three digits[2].

Let us remark that our specific predictions are validated by well-tested approaches such as the view factors (see e.g. the standard [21]). Although our specific results, e.g. the location of maximum t_{op} for strip heaters, pertain to a well-defined problem in our configuration (that is, the test room without openings), here we have shown quantitatively two general features: how the radiator performance changes with panel area, and the existence of optimal sizes for the UFH and ceiling heater.

Additionally, our analytical study introduces a simple predictive method for computing the operative temperature for *any* panel size and radiator type, as it can be easily applied to sizes and enclosures which are different from those considered here. For the case at hand, we list a series of analytical formulas for calculating t_{op} for radiators of 10- or 21-type, with panel size in the range considered and excluding back wall losses.[3]

---

1 We will show that the t_{op} obtained this way is not radically different from the analytical result.
2 In theory one might conclude that the UFH is the ideal heater, but in practical cases the embedded emission losses are relevant [8].
3 Adiabatic internal surfaces are used in the model, namely no additional heat is transferred from the ceiling heater and UFH to the colder rooms above and below. This additional heat loss is also omitted for the radiators, to guarantee an accurate comparison.

 doi:10.20944/preprints201809.0142.v2

The present paper is organized as follows: in Section 2 we describe the test chamber, the simulation setup and the different methods for computing the operative temperature. In Section 3 we report our results for each single case, while Section 4 contains a summary of our findings and concluding remarks. In the Appendix we report considerations about the view factors, a comparison between our analytical and numerical methods and the analytical formulas to determine the operative temperature for any radiator size.

2. Method

In this study, we consider an enclosure with thermal layer properties and dimensions 4mx4mx3m specified by the CEN TC130 European Committee, shown in Figure 2. The external wall has U-value 0.25 W/m2K, and the room was ventilated with heat recovery ventilation providing an air change rate of 1 ACH.

Vertical temperature gradients are mainly influenced by the amount of air circulation within an enclosure. As it was shown in [8], gradients measured for radiators and UFH were approximately 0 K/m for ventilated rooms. The ventilation flow rates and room geometry (mainly the height of the room) within the referenced study are similar to the room considered in this paper. We accordingly neglect the possible effects of a vertical temperature gradient, assuming indoor air mixing and lack of stratification to be similar. This approximation is therefore true at least for radiators and UFH, however no information exists for ceiling heater. We do note that including a vertical gradient would yield marginally different surface (and thus operative) temperatures, since the temperature differences for convection calculation purposes would change between the room air and enclosing surfaces only slightly. A more detailed study on this phenomenon would certainly be interesting, however it would require extensive measurements to accurately assess the variation in the gradient values, as the size of the emitters changes within a broad range.

We locate the calculation point, namely the centre of mass of an average sitting user, at 0.6m above the floor in the room centre (i.e., at 2m distance from each wall) [21]. The most performing heater configuration will then be the one providing the highest operative temperature, with the same heater nominal output. The steady-state boundary conditions are the following: Indoor air temperature T_{in}=20 °C, external air temperature T_{ext}= -15°C. Both direct normal and diffuse horizontal irradiance are set to zero. 134 W of power are required to heat up the room under these predefined conditions (the heat outputs throughout the simulations were within $\pm$0.5 W of this value).

IDA-ICE calculates the heat emission from any hydronic heating device as follows. The characteristic equation used to determine and model the device's heat output comes in the form of an empirical power law [25],

$$P = kldT^n\,, \tag{1}$$

where k and n are coefficients determined individually for each emitter type, with l its length and dT the logarithmic mean temperature difference between heating water and indoor air. This governing equation therefore holds true for radiators, ceiling panels and UFH. The detailed version of the model, containing the heat balance equations used in the IDA ICE software for e.g. the calculation of relevant flow and surface temperatures, can be found in [26].

For underfloor heating, the pipe installation depth and the fluid-to-slab heat transfer coefficient are provided by the user along with the nominal heat output P_{nom} at a given temperature drop ΔT_{nom} for the underfloor heating system. The maximal mass flow G_{max} through the underfloor piping is then calculated as

$$G_{max} = \frac{P_{nom}}{\Delta T_{nom} c_p}\,, \tag{2}$$

where c_p is the specific heat capacity of water at constant pressure. The exact heat output, return temperature and mass flow depend on the actual amount of heat required within the room.

Heat transfer from the heating water to the surfaces of heating pipe and floor is modelled with an n-layered RC-network, see [26] for exact model descriptions. The piping layer is basically given by

Preprints (www.preprints.org) | NOT PEER-REVIEWED | Posted: 6 November 2018 doi:10.20944/preprints201809.0142.v2

a heat exchanger, with an active plane at constant surface temperature located inside the floor slab. In the resulting floor coil model, the heat transfer between fluid and active plane is computed via their logarithmic temperature difference; the according heat transfer coefficient includes convection between medium and tube wall, heat conduction through the tube walls and "fin efficiency" given by the distance between immersed tubes or actual fins. In steady state, this approach corresponds to the resistance method of the EN 15377-1 standard [27].

For a selection of IDA ICE model and software validations, see e.g. [28–32].

The operative temperature t_{op} is computed analytically, according to the prescriptions of the ISO 7726 standard, as we explain in the following. Considering the contributions of all the six surfaces in the enclosure, we obtain an expression for $t_{op} = t_{op}(a, b)$ that is a function of the radiator height a and width b. The eventual global maxima of this function in the (a, b) plane would then correspond to the optimal configuration for that specific heater. Such full analytical solution is then numerically validated by the finite difference method software IDA ICE [22] in the same CEN TC130 test room, in the limit when only the contribution of the surfaces that are parallel to the principal calculation surface is accounted for.

The operative temperature at the above location is not uniquely defined. In IDA ICE this is evaluated as the simple arithmetic average of air temperature t_{air} and mean radiant temp. $\bar{t}_r$ [22],

$$t_{op} = \frac{t_{air} + \bar{t}_r}{2}\,, \tag{3}$$

(throughout this paper, $[t_i]$=[°C] and $[T_i]$=[K]). This differs from the exact definition given in the ISO 7726 [21],

$$t_{op} = \frac{h_c t_{air} + h_r \bar{t}_r}{h_c + h_r} \equiv A t_{air} + (1 - A)\bar{t}_r\,, \tag{4}$$

where the average is weighted by the radiation and convection heat transfer coefficients h_r and h_c at the calculation point[4]. The explicit formula for the coefficient A, which is itself a function of h_c and h_r, is given in the Appendix; for our setup, it lies within the range $A \sim 0.5 - 0.6$.

Another difference between the ISO standard and IDA ICE is that the numerical software has a peculiar way of computing the mean radiant temperature $\bar{t}_r$. It considers only the surfaces that are *parallel* to the principal calculation surface, therefore the sum of view factors in a principal direction is < 1 (Figure 4). Moreover, $\bar{t}_r$ is obtained as the average of mean radiant temperatures from the six principal directions, weighted by the respective view factors,

$$\overline{T}_{mrt} = \sqrt[4]{\frac{\sum_{i=1}^{6}\sum_{j=1}^{n} F_{i\to j} T_j^4}{\sum_{i=1}^{6}\sum_{j=1}^{n} F_{i\to j}}}\,, \tag{5}$$

where the $F_{i\to j}$ are computed for a small area (the observer) that is only parallel to the radiating surface.

In contrast, the ISO 7726 prescribes that for each direction one considers both parallel *and* perpendicular surfaces (see Figure 5), obtaining the plane radiant temperature [14,21],

$$\overline{T}_{pr}^{(i)} = \sqrt[4]{\sum_{j=1}^{6} F_{p-A_j} T_{sj}^{(i)4}}\,, \tag{6}$$

[4] As we demonstrate in the Appendix, in reality the different operative temperature values which are obtained with either method show no sizeable difference.

Preprints (www.preprints.org) | NOT PEER-REVIEWED | Posted: 6 November 2018 doi:10.20944/preprints201809.0142.v2

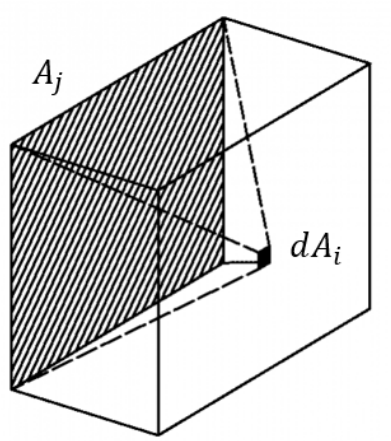

Figure 4. Calculation of mean radiant temperature from IDA-ICE [22].

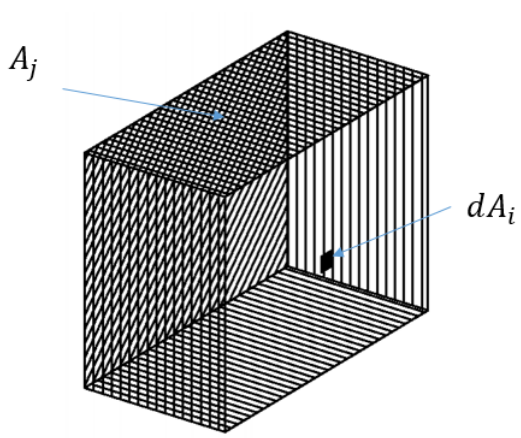

Figure 5. Calculation of mean radiant temperature from ISO 7726 [21].

with the angle factors F_{p-A_j} reported in the Appendix. Now the sum of view factors in each direction is accordingly =1, and the mean radiant temperature is given by [21],

$$\bar{t}_r(a,b,c) = \sqrt[4]{\frac{\sum_{i=1}^{6} \beta_i \overline{T}_{pr}^{(i)}(a,b,c)}{\sum_{i=1}^{6} \beta_i}} - 273.15, \tag{7}$$

namely by a weighted average over the projected area factors β_i of a person, listed in Table 1.

Table 1. Projected area factors of a person [21].

	Standing	Seated
Up/down	0.08	0.18
Left/right	0.23	0.22
Front/back	0.35	0.30

Specifically, in this work all the "Analytical Full" t_{op} points in the graphs are calculated with Eqs.(4) and (7), therefore following the ISO standard completely throughout this paper. The only point in common with IDA ICE consists of the surface temperatures $T_{sj}^{(i)}$, which are written as polynomial interpolations from the data provided by the software. Since both the definitions of operative and mean radiant T are different, the analytical t_{op} is independent of the numerical t_{op}.

On the other hand, for the "Analytical as IDA ICE" points, while still computing analytically, we use Eqs.(3) and (5), consistently with the software. This provides validation of both our view factors and the temperature interpolations $T_{sj}^{(i)} = T_{sj}^{(i)}(x)$, where x is a length that is specific to the particular case (either a or b). The interpolations are implemented towards a more general form of the operative temperature than by using the raw data for the surface temperatures. This way, instead of calculating t_{op} for each point, we can write $t_{op} = t_{op}(x)$ and accordingly formulate general considerations and predictions on the operative temperature for *any* possible configuration consistent with the test room setup. In the case of UFH and ceiling heater, the "square" configuration consists of a square heater placed under the floor or ceiling surface, centred in the middle of the room, where the user is sitting. The "strip" configuration instead considers a heated strip running from the cold (or external) wall. Further descriptions are given in Sections 3.2 and 3.3.

Preprints (www.preprints.org) | NOT PEER-REVIEWED | Posted: 6 November 2018 doi:10.20944/preprints201809.0142.v2

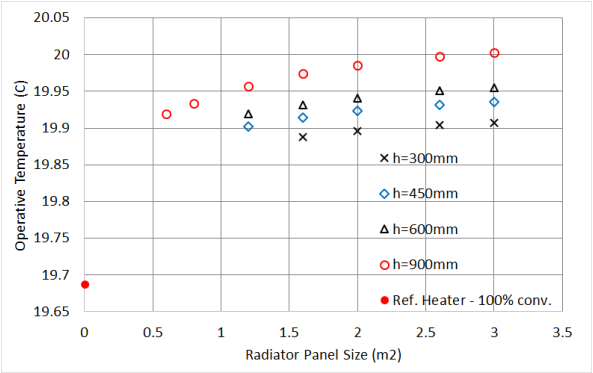

Figure 6. IDA ICE operative temperatures for a 10-type radiator and convector in function of the panel area.

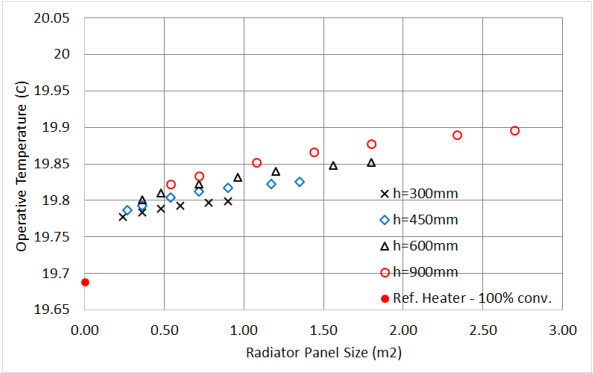

Figure 7. IDA ICE operative temperatures for a 21-type radiator and convector in function of the panel area.

3. Results and Discussion

3.1. Panel radiator

As discussed in the previous section, in this study we consider a room with a single external wall and adiabatic internal walls, floor and ceiling under steady-state conditions. Thermal layer properties and room dimensions (Figure 2) are chosen according to the European CEN technical committee TC130 working group WG13 specifications, with a U-value for the external wall U=0.25 W/m2K. A supply temperature of 55°C was used. Different types and sizes of heat emitters (radiators, UFH and ceiling heater) are used in IDA ICE simulations to offset the heat loss through the external wall (specific details for each emitter type are presented in their relevant sections). The resulting surface temperatures as calculated by the software are logged and used as input in the analytical calculation. The operative temperatures computed by IDA ICE are also used for comparison with the analytical result.

Figures 6 and 7 illustrate first of all that the area by itself is not a good parameter for assessing the performance: given the same area, the efficiency varies with height. Additionally, and more importantly, we observe that one cannot identify a reference ideal convector with 100% convection and 0% radiation as an ideal heater, since it returns the lowest operative temperature.

Operative temperatures for fixed heights are plotted in Figures 8 and 9. These hold respectively for a 10-type and a 21-type panel radiator (some values for the 10-type are missing, as it could not reach 134W of power output). One can see that in general, the numerical and analytical solutions are nearly equivalent. Only for the 10-type we see a slight deviation; moreover, the 10-type reveals to be the most performing radiator, with t_{op} values always exceeding those of the 21-type by $\sim$0.1°C . They can even approach the air temperature 20°C at $h = 0.9$m. We can thus conclude that for the study at hand the 10-type can be identified as our "ideal" radiator.

Further conclusions can be made rigorous by means of our analytical solution. First of all, the t_{op} values are linearly distributed along different heights h. By applying a method first introduced in [24], we interpolate the operative temperature versus the height (minimum square method), for a fixed width. The according curves can be generally written as

$$t_{op}(h, w) = A(w)h + B(w)\,, \tag{8}$$

returning the operative temperature in the range $0.3m \leq h \leq 0.9m$, for *any* desired height h, by using the explicit formulas listed in Tables A1 and A2.

Preprints (www.preprints.org) | NOT PEER-REVIEWED | Posted: 6 November 2018 doi:10.20944/preprints201809.0142.v2

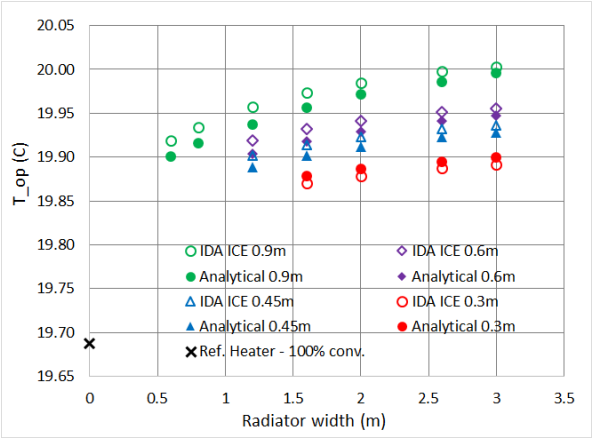

Figure 8. Operative temperatures for a 10-type panel radiator, with $h = 0.3, 0.45, 0.6, 0.9$m.

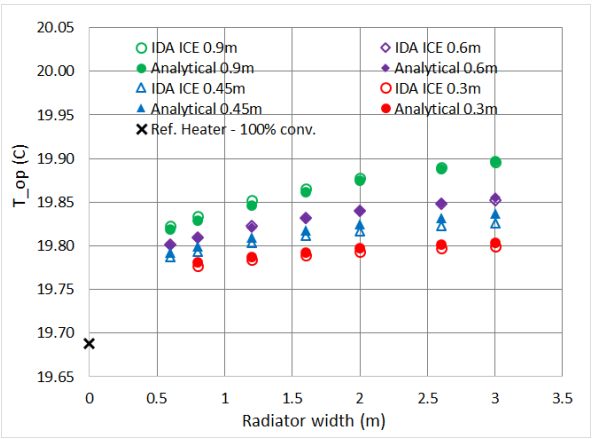

Figure 9. Operative temperatures for a 21-type panel radiator, with $h = 0.3, 0.45, 0.6, 0.9$m.

In contrast, assuming a given height provides t_{op} values that are *not* linearly distributed along different widths w. They rather follow a quadratic law in the form

$$t_{op}(h, w) = A(h)w^2 + B(h)w + C(h)\,. \tag{9}$$

As it is shown in Tables A3 and A4, one finds $A(h) < 0$ for any height. t_{op} grows instead linearly with increasing height, $t_{op}(h, w) = A(w)h + B(w)$ with $A(w) > 0$ (Tables A1 and A2): this verifies the physical result that the operative temperature is more dependent on the height than on the width[5].

The analytical solution allows to make even more specific conclusions. As an example, consider the 21-type radiator. The explicit form of the operative temperature is generally highly non linear, however plotting the first derivative $Dt_{op} \equiv dt_{op}/dw$ in function of the width returns additional information. In Figure 10 we find indeed a "plateau" starting at $w \sim$1m and ending at about 2m, where the decrease with w is less pronounced: in other words, in the according range Δw the operative temperature t_{op} is optimised with respect to width increase, and widths contained in this interval are most advantageous.

The approximated range Δw above is probably precise enough for practical applications, however an analytical formula such as Eq.(9) allows to identify its boundaries with high precision. The second and third derivatives $D^2t_{op} \equiv d^2t_{op}/dw^2$ and $D^3t_{op} \equiv d^3t_{op}/dw^3$ provide indeed the exact locations of the plateau, at $w = 0.87$m and $w = 1.86$m respectively . The latter point corresponds to a minimum of D^3t_{op}, which identifies a change of concavity in D^2t_{op}. Finally, the second derivative gives the exact point of minimal increment of t_{op}, sitting at $w = 2.736$m. Interestingly, exactly the same value holds for $h = 0.9$m, as illustrated in Figure 11.

To summarize, investigating the performance of 10- and 21-type panel radiators we have rigorously proven that

- given the same area, the efficiency varies with height,
- an ideal convector with 100% convection performs worse than panel radiators,
- the 10-type can be identified as our ideal heater,
- the operative temperature is more dependent on the height than on the width,
- there exists an ideal width range for 21-type radiators.

---

5 One can also prove that Eqs.(8) and (9) are equivalent, namely by substituting one value for h and w they return the same t_{op} (discrepancy of order ~ 0.001, around 0.02%).

Preprints (www.preprints.org) | NOT PEER-REVIEWED | Posted: 6 November 2018 doi:10.20944/preprints201809.0142.v2

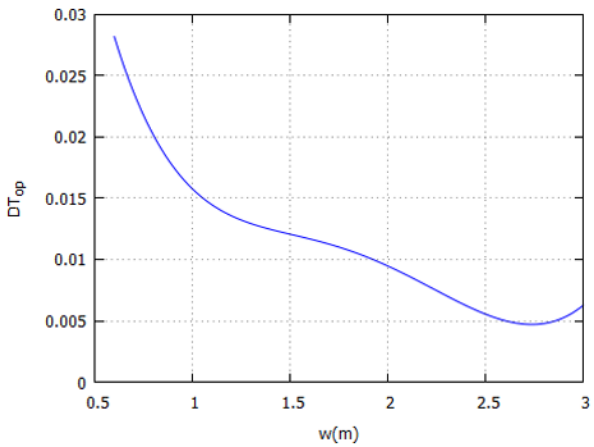

Figure 10. First derivative of the analytical operative temperature for a 21-type radiator, $h = 0.3$m.

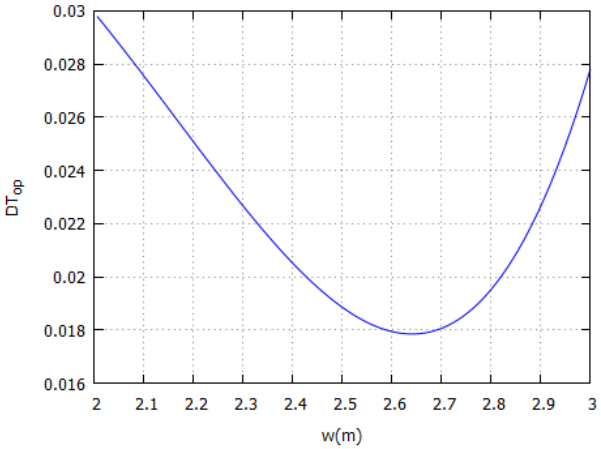

Figure 11. First derivative of the analytical operative temperature for a 21-type radiator, $h = 0.9$m.

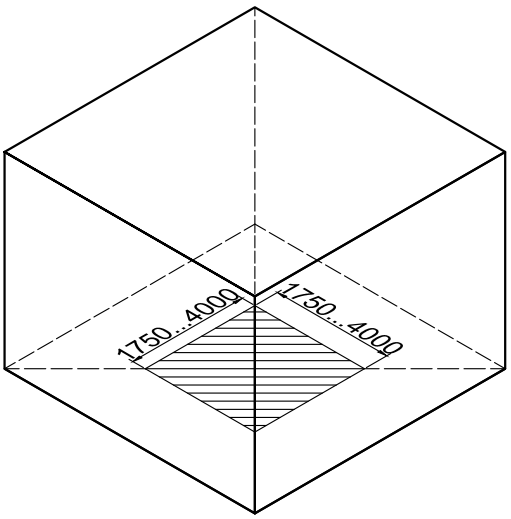

Figure 12. Underfloor heating - square setup

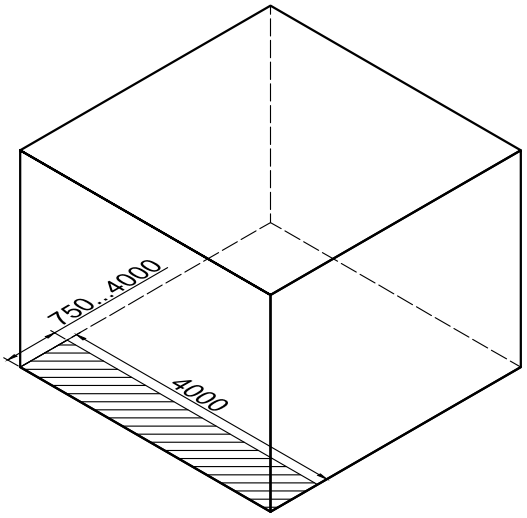

Figure 13. Underfloor heating - strip setup

Furthermore, we provide in Tables A1 to A4 useful analytical formulas which determine precisely the operative temperatures for any width and height in the ranges considered in the study at hand.

3.2. Underfloor heating

Regarding underfloor heating (UFH), we considered two different cases: a square heater in the centre of the floor, with varying side length (Figure 12), and a strip setup with fixed width as the floor and varying depth from the external wall (Figure 13). A nominal heat output of 50 W/m2 at a water-side temperature drop of $\Delta T = 7K$ was used as input for the IDA ICE model, with the piping placed at 25mm depth in screed. A 30 W/m2K fluid-to-slab heat transfer coefficient and a supply temperature of 35°C were used.

The operative temperature for square and strip UFH is plotted in Figs.14 and 15 respectively. Here we compare IDA ICE (dots) with an analogous analytical calculation with no projection on perpendicular surfaces (crosses) and with the full analytical calculation (all the 6 directions with perpendicular surfaces), diamonds.

In both cases the analytical model agrees with the numerical computation with an excellent precision. Notice however how the full solution deviates by ~ 0.1°C from IDA ICE unless the square

Preprints (www.preprints.org) | NOT PEER-REVIEWED | Posted: 6 November 2018 doi:10.20944/preprints201809.0142.v2

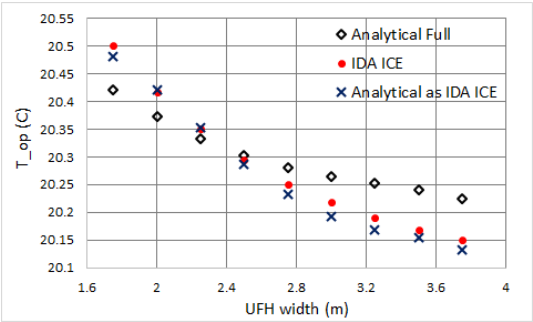

Figure 14. Operative temperature for a square UFH.

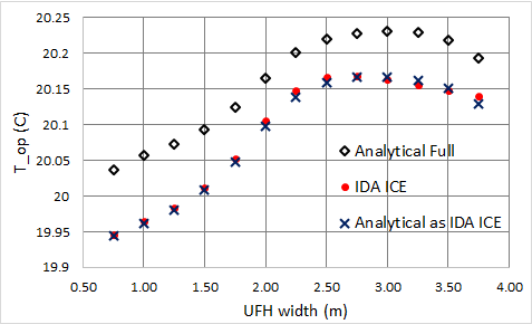

Figure 15. Operative temperature for a strip UFH.

width is around 2m: considering the horizontal and vertical walls as a whole, this case corresponds to the most symmetric configuration indeed. As it can be seen by investigating the view factors of each surface, for smaller squares $w < 2$m IDA ICE does not account for the heat dissipation to the vertical walls[6]. On the other hand, for $w > 2$m these contribute to increasing t_{op} at the calculation point (2m from each wall, at 0.6m from the floor). The main result in any case is that there is no evident optimal size for the UFH with this configuration.

In the case of UFH as a strip running between the side walls, starting from the cold wall, we find instead something more interesting. Neglecting the vertical walls we get again an excellent cross-check with IDA ICE; furthermore, the extension to the full enclosure shows a systematic difference of nearly 0.1°C, accounting for the effect of vertical walls. While qualitatively there is basically no deviation from the numerical solution, this is interesting when considering precision calculations.

More importantly, we find a very distinct maximum for t_{op} between 3m and 3.1m, Figure 15. By means of the analytical form of the solution, we can compute its location precisely at $w = 3.0372$m, see Fig.20. Notice also that, qualitatively, the operative temperature difference between radiators and a fully covering UFH is comparable to that obtained in the experimental paper [8].

3.3. Ceiling heater

The two configurations of square and strip heaters we addressed for floor heating were also considered for the ceiling (Figures 16 and 17). Geometrically, the setup is a mirror-reflection of the floor model on the vertical axis. The main difference in the view factors is in the calculation point, which now sits at 2.4m from the heated surface, making the reflection not perfectly symmetrical. Catalogue values of a well-known manufacturer were applied for the IDA ICE model input (nominal heat output of 529.2 W/m^2 at $\Delta T_{ln} = 50K$ with characteristic exponent n=1.174). A supply temperature of 45°C was used. The operative temperatures in this case are given in Figures 18 and 19, and the absolute maximum for a heated strip is shown in Fig.21. It occurs at $x = 3.1349$m.

Comparing Figure 18 with Fig.14, we notice a marginal difference for $w < 2m$, while otherwise the same higher t_{op} with respect to IDA ICE is obtained. The operative temperature values are naturally smaller in this case, due to the larger distance heater-observer that reduces the heat transfer. For a heated strip, this is reflected in Figure 19, showing a smaller effect of the vertical walls compared to Figure 15. Qualitative differences are irrelevant.

4. Conclusions

Thermal comfort is strictly related to the energy efficiency of heating systems in buildings, and it can be quantified by the operative temperature t_{op}, namely the temperature sensed by the user. In

[6] These lower values hold also if one uses the IDA ICE data directly, therefore they are not due to errors related to the interpolations of the surface temperatures.

Preprints (www.preprints.org) | NOT PEER-REVIEWED | Posted: 6 November 2018 doi:10.20944/preprints201809.0142.v2

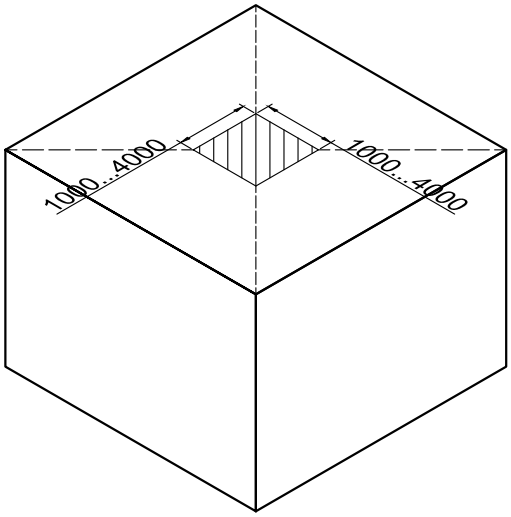

Figure 16. Ceiling panel - square setup

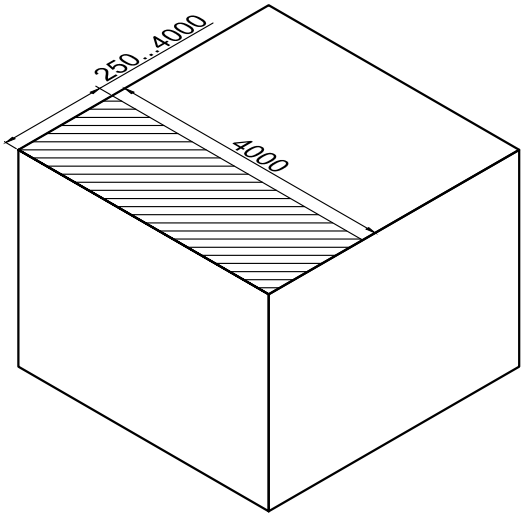

Figure 17. Ceiling panel - strip setup

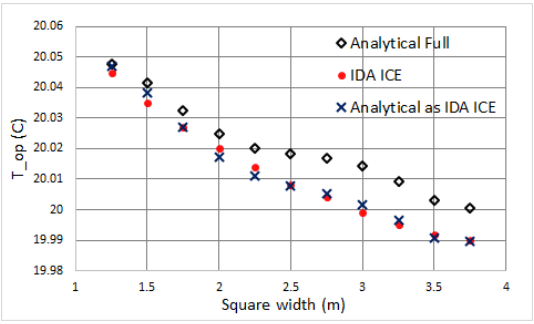

Figure 18. Operative temperature for a heated square portion of the ceiling.

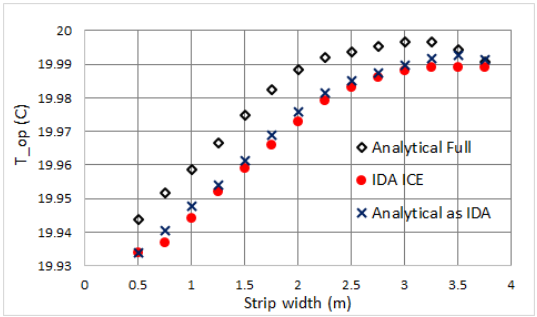

Figure 19. Operative temperature for a heated strip on the ceiling.

this paper we performed a rigorous investigation of the operative temperature induced on users by several types of different heat emitters, in the search for the most performing, or ideal, heater. We considered a number of configurations of practical interest, with analytical and numerical calculations of t_{op} performed in a test room with a standard size defined by updated European Standards.

Specifically, considering panel radiators, underfloor and ceiling heaters, we obtained the general behaviour of the operative temperature as a function of emitter type, size and room geometry. We addressed panel radiators of 10- and 21-type installed on the cold wall, for a variety of sizes and surface temperatures. Compared with an ideal convector providing the same output $\sim$ 134W, we found the 10-type to be the most performing radiator. For larger sizes, the 10-type is even capable to induce an operative temperature that is equal to the air temperature 20°C. This means that it constitutes our "ideal" radiator for the setup considered in this paper.

Via our analytical calculations we were able to draw a number of considerations, proving for instance that the performance of radiators is more sensitive to the height than to the width, and providing according exact formulas. These can be of practical use for radiators of 10- or 21-type with dimensions $0.3m \leq h \leq 0.9m$ and $1.2m \leq w \leq 3m$, assuming no back wall losses; they are listed in Tables A1 to A4. Furthermore, in the case of 21-type panel radiators we also highlighted a width interval for which adopting larger panels is most convenient, as it contains a size range that is optimal for the operative temperature.

For underfloor UFH and ceiling heater strips, we identified the occurrence of non-trivial global maxima, corresponding to the highest temperature sensed by a person sitting in the middle of the room. If a UFH heated square could follow and track an occupant location, this solution would represent

Preprints (www.preprints.org) | NOT PEER-REVIEWED | Posted: 6 November 2018 doi:10.20944/preprints201809.0142.v2

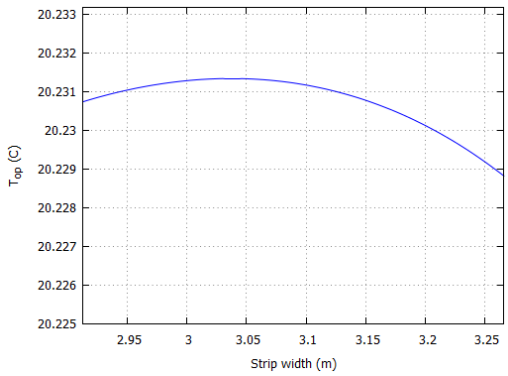

Figure 20. Operative temperature maximum for a strip heated area underfloor.

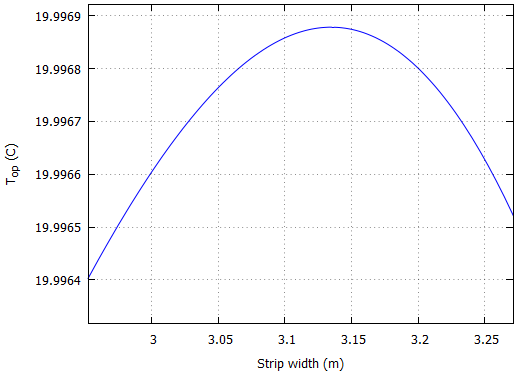

Figure 21. Operative temperature maximum for a heated strip on the ceiling.

the best performing heater with the highest operative temperature, a result that may have practical implications for personal thermal comfort solutions.

Also, via the systematic difference between numerical and analytical values shown in our plots, one could quantify precisely the effect of the vertical walls, which are ignored in the numerical calculation. The difference, though rather small, is however sizeable.

We notice that the ceiling heater t_{op} is very close to the 10-type radiator, and that the UHF optimal strip measuring 3/4 of the room width may correspond to our overall ideal heater, since it provides a 0.23 K higher op.temp. than the 10-type radiator[7]. Furthermore, compared to typical radiator sizes with height 0.6m, the UFH provides 0.25 K - 0.3 K higher t_{op} relative to the 10-type and 0.35 K relative to the 21-type.

The fact that the op.temp. approaches the air temperature is very advantageous for energy saving, as it was shown e.g. in [33] that the energy demand is very sensitive to operative temperature corrections. In particular, a difference of only 0.1°C is capable of inducing an increase in the annual heating need by 1-2% [33]: such effect is found for the convector and 21-type panel radiator, which are therefore fairly underperforming. Specifically, the former shows the worst performance: the op.temp. is lower by 0.55 K when compared to UFH. This is in agreement with Table 2, which shows the surface temperatures in the enclosure for the smallest size of each emitter type addressed in this study.

However, the air and operative temperature differences calculated in this study should not be directly applied for energy saving assessment, because they are valid at the outdoor temperature -15°C, which is much lower than the average heating season value. As the differential between outdoor and indoor air temperature decreases, we expect the corresponding $\Delta t = t_{air} - t_{op}$ to decrease as well, since each and every wall surface temperature tends to approach the indoor air T. Also the emitters' surface temperatures will decrease, affecting the mean radiant T and therefore t_{op} accordingly. In other words, for a more realistic (higher) outdoor temperature we expect Δt to be generally smaller than what reported in this study.

The investigation presented in this paper constitutes a good starting point for a number of improvements in the search for an ideal heater. First of all, parametric studies on the relationship between view factors, room and geometry of the emitter might show a more general pattern, whose impact on the whole energy demand could be quantified with e.g. annual simulations.

Funding: The research was supported by the Estonian Research Council with Institutional research funding grant IUT1-15. The authors are also grateful to the Estonian Centre of Excellence in Zero Energy and Resource Efficient

[7] Clearly, though the UFH and ceiling smallest squares provided the highest operative temperature, such cases are not realistic, because a small square heater cannot track the occupants when they move around the room.

Preprints (www.preprints.org) | NOT PEER-REVIEWED | Posted: 6 November 2018 doi:10.20944/preprints201809.0142.v2

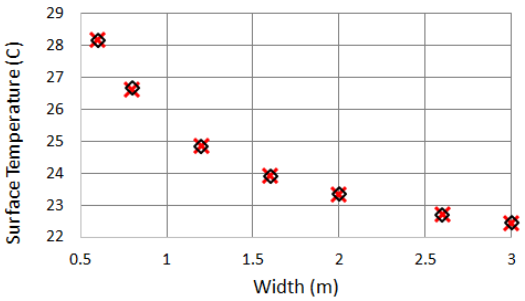

Figure A1. Comparison of surface temperatures for a 21-type radiator, $h = 0.9m$. IDA ICE (crosses) vs 4th order polynomial interpolation (diamonds).

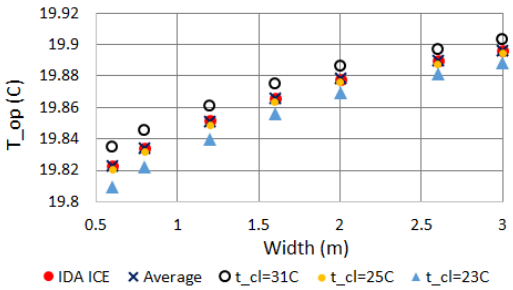

Figure A2. Operative temperatures for a 21-type, IDA ICE cross-check: arithmetic (crosses) vs weighted average for different clothing surface temperatures.

Smart Buildings and Districts, ZEBE, grant 2014-2020.4.01.15-0016 funded by the European Regional Development Fund.

Conflicts of Interest: The authors declare no conflict of interest.

Appendix View factors and operative temperature formulas

The view factors for a small area parallel or perpendicular to a surface of height a and width b, separated by a distance c, hold respectively as [21]

$$F_{p-A_i} = \frac{1}{2\pi}\left(\frac{X}{\sqrt{1+X^2}}\arctan\frac{Y}{\sqrt{1+X^2}} + (X \leftrightarrow Y)\right), \tag{A1}$$

with $X = a/c, Y = b/c$, and

$$F_{p-A_i} = \frac{1}{2\pi}\left(\arctan\frac{1}{Y} - \frac{Y}{\sqrt{X^2+Y^2}}\arctan\frac{1}{\sqrt{X^2+Y^2}}\right), \tag{A2}$$

with $X = a/b, Y = c/b$. We should remark that the calculation of mean radiant temperatures for the perpendicular surfaces is extremely sensitive to how the above view factors are implemented. For example, in Section 3.1 we discussed panel radiators of varying height h that are installed on the cold wall, at 15cm from the floor. In this case, one could naively compute the view factor from the lower edge of the cold wall up to the top of the radiator ($a = h + 15cm$), or alternatively ignoring the 15cm displacement ($a = h$). It can be shown that the view factor differs critically for both cases and returns a non physical result for the operative temperature.

The reason is that the above functions are not linear in a, b, c: since the view factors are additive, a more correct way to calculate them with formulas (A1) and (A2) consists of subtracting F_{p-A_i} at $a = h$ from F_{p-A_i} at $a = h + 15cm$. This way one obtains a *net* view factor, which despite not being 100% accurate, returns physical operative temperatures that match earlier results [20,33] and the present numerical simulations (see e.g. Figs. 18 and 19).

We conclude with a few considerations about the definition of operative temperature adopted in this paper. In Section 2 we remarked that IDA ICE uses the simple arithmetic average of air temperature

Table 2. Emitter and room surface temperatures [°C] for minimal sized emitters.

Emitter type	Emitter surf.	Floor	Ceiling	Sidewalls	Backwall	External wall
10-type radiator	33.83	19.78	19.80	19.72	19.74	18.59
21-type radiator	32.04	19.61	19.71	19.60	19.62	18.53
UFH, square	24.66	19.89	20.03	20.01	20.03	18.92
Ceiling heater, square	31.78	20.00	19.90	19.95	19.96	18.87

Preprints (www.preprints.org) | NOT PEER-REVIEWED | Posted: 6 November 2018 doi:10.20944/preprints201809.0142.v2

t_{air} and mean radiant temperature $\bar{t}_r$, Eq.(3). On the other hand, for the analytical calculation we used the exact formula for computing the op.t., Eq.(4). The A coefficient is expanded as

$$A \equiv \left(1 + \frac{h_r}{h_c}\right)^{-1}, \tag{A3}$$

and we express h_c and h_r in function of the air and mean radiant temperatures by means of the following [34–36]: the heat transfer coefficient for radiation is written as

$$h_r = \sigma \epsilon_{cl} \frac{A_r}{A_D} \frac{(t_{cl} + 273.15)^4 - (\bar{t}_r + 273.15)^4}{t_{cl} - \bar{t}_r}, \tag{A4}$$

where ϵ_{cl} is the emissivity of a clothed person and A_r/A_D the ratio of the body radiation area (0.67 for crouching, 0.7 for sitting and 0.73 for standing). ϵ_{cl} lies typically in the range 0.8-0.9 [37], here we use ϵ_{cl}=0.9. It can be shown that a 0.1 difference in the emissivity is marginal to the operative temperature, inducing an $\mathcal{O}(0.001)$ difference in t_{op}, which is less than 0.1%. The same holds for the ratio A_r/A_D, as it is evident from Eq.(A4); in this paper we choose $A_r/A_D = 0.7$. $\sigma = 5.67 \times 10^{-8}$W/(K^{4}m2) is the Stefan-Boltzmann constant.

The convection coefficient holds instead as

$$h_c = 2.38 \sqrt[4]{t_{cl} - t_{air}}, \tag{A5}$$

if $2.38 \sqrt[4]{t_{cl} - t_{air}} > 12.1 \sqrt{V_{air}}$, otherwise

$$h_c = 12.1 \sqrt{V_{air}}, \tag{A6}$$

with V_{air} [m/s] the air velocity relative to the human body. Since for our room the air ventilation rate is 1 ACH, V_{air} is very small, of $\mathcal{O}(0.01)$ m/s, therefore we use Eq.(A5).

The clothing surface temperature for a sitting person doing office work can vary depending on the clothing; moreover, the exact calculation is rather involved and based on a recursive formula [36]. Considering three cases $t_{cl} = 23, 25, 31$°C, which are shown in Figure A2, one can see a small impact of t_{cl} on t_{op}. In particular, $t_{cl} = 25$°C reproduces the IDA ICE values almost exactly.

The operative temperature evaluated (ideally) on the surface of a clothed user is thus a function of air and mean radiant temperatures, and of the heat transfer coefficients measured at that same point. As $\bar{t}_r = \bar{t}_r(a, b, c)$, also the radiation coefficient h_r in (A4) is a function of the radiator dimensions a and b, together with the distance radiator-person c.

Comparison of the operative temperature as computed with (4), namely with h_r and h_c instead of the arithmetic average (3) for $t_{cl} = 25$°C is illustrated in Fig.A3.

It can be easily verified that for underfloor and ceiling heater the t_{op} difference is even more negligible (of the order ~ 0.01°C). Figure A1 also shows the precision of the interpolations used in this paper for a type-21 panel radiator.

One might also wonder about the effect of (4) on the cross-check with IDA ICE, namely when computing the mean radiant temperature without considering the heater projections on the perpendicular surfaces. The result is given in Figure A2.

Quite interestingly, as a last remark, we note that by shifting the point for the calculation of view factors on the surfaces perpendicular to the radiator, one can cancel their effect and recover the IDA ICE result with accuracy close to ~ 0.01. This curious coincidence perhaps recalls to mind the role of inertial observers in Newtonian mechanics.

Preprints (www.preprints.org) | NOT PEER-REVIEWED | Posted: 6 November 2018 doi:10.20944/preprints201809.0142.v2

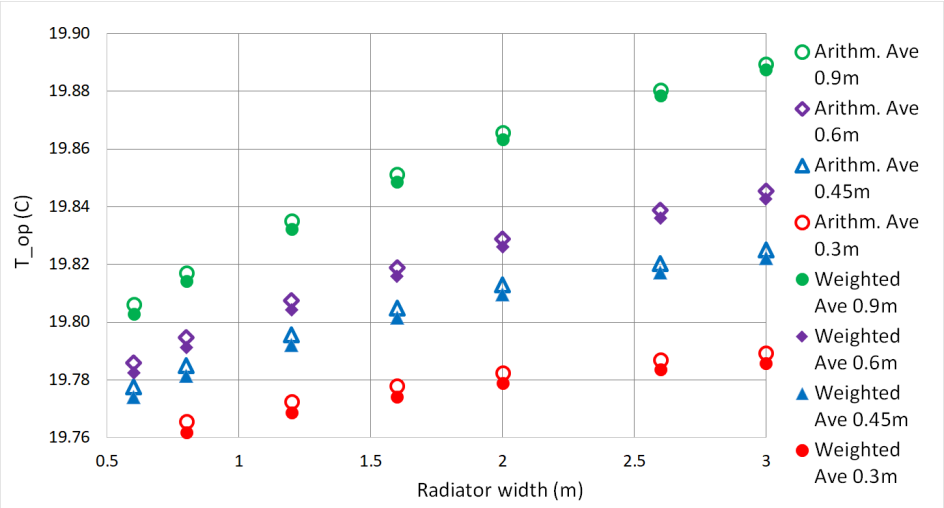

Figure A3. Operative temperatures for a 21-type panel radiator, arithmetic average Eq.(3) vs average weighted with convection and radiation coefficients (*A*-factor in Eq.(4)).

References

1. Serrano, S.; Ürge Vorsatz, D.; Barreneche, C.; Palacios, A.; Cabeza, L.F. Heating and cooling energy trends and drivers in Europe. *Energy* **2017**, *119*, 425 – 434. doi:https://doi.org/10.1016/j.energy.2016.12.080.
2. D'Agostino, D.; Cuniberti, B.; Bertoldi, P. Data on European non-residential buildings. *Data in Brief* **2017**, *14*, 759 – 762. doi:https://doi.org/10.1016/j.dib.2017.08.043.
3. Yao, R.; Steemers, K. A method of formulating energy load profile for domestic buildings in the UK. *Energy and Buildings* **2005**, *37*, 663 – 671. doi:http://dx.doi.org/10.1016/j.enbuild.2004.09.007.
4. Olesen, B.W.; Mortensen, E.; Thorshauge, J.; Berg-Munch, B. Thermal comfort in a room heated by different methods. *ASHRAE transactions* **1980**, *86*, 34–48.
5. Inard, C.; Meslem, A.; Depecker, P. Energy consumption and thermal comfort in dwelling-cells: A zonal-model approach. *Building and Environment* **1998**, *33*, 279 – 291. doi:https://doi.org/10.1016/S0360-1323(97)00074-7.
6. Olesen, B.W.; de Carli, M. Calculation of the yearly energy performance of heating systems based on the European Building Energy Directive and related CEN standards. *Energy and Buildings* **2011**, *43*, 1040 – 1050. Tackling building energy consumption challenges - Special Issue of ISHVAC 2009, Nanjing, China, doi:https://doi.org/10.1016/j.enbuild.2010.10.009.
7. Léger, J.; Rousse, D.R.; Borgne, K.L.; Lassue, S. Comparing electric heating systems at equal thermal comfort: An experimental investigation. *Building and Environment* **2018**, *128*, 161 – 169. doi:https://doi.org/10.1016/j.buildenv.2017.11.035.
8. Maivel, M.; Ferrantelli, A.; Kurnitski, J. Experimental determination of radiator, underfloor and air heating emission losses due to stratification and operative temperature variations. *Energy and Buildings* **2018**, *166*, 220 – 228. doi:https://doi.org/10.1016/j.enbuild.2018.01.061.
9. Võsa, K.V.; Ferrantelli, A.; Kull, T.M.; Kurnitski, J. Experimental analysis of emission efficiency of parallel and serial connected radiators in EN442 test chamber. *Applied Thermal Engineering* **2018**, *132*, 531 – 544. doi:https://doi.org/10.1016/j.applthermaleng.2017.12.109.
10. Myhren, J.A.; Holmberg, S. Performance evaluation of ventilation radiators. *Applied Thermal Engineering* **2013**, *51*, 315 – 324. doi:https://doi.org/10.1016/j.applthermaleng.2012.08.030.
11. Risberg, D.; Risberg, M.; Westerlund, L. CFD modelling of radiators in buildings with user-defined wall functions. *Applied Thermal Engineering* **2016**, *94*, 266 – 273. doi:https://doi.org/10.1016/j.applthermaleng.2015.10.134.
12. Hasan, A.; Kurnitski, J.; Jokiranta, K. A combined low temperature water heating system consisting of radiators and floor heating. *Energy and Buildings* **2009**, *41*, 470 – 479. doi:https://doi.org/10.1016/j.enbuild.2008.11.016.

13. Ali, A.H.H.; Gaber Morsy, M. Energy efficiency and indoor thermal perception: a comparative study between radiant panel and portable convective heaters. *Energy Efficiency* **2010**, *3*, 283–301. doi:10.1007/s12053-010-9077-3.
14. Kalmár, F.; Kalmár, T. Interrelation between mean radiant temperature and room geometry. *Energy and Buildings* **2012**, *55*, 414 – 421. doi:https://doi.org/10.1016/j.enbuild.2012.08.025.
15. Shati, A.; Blakey, S.; Beck, S. The effect of surface roughness and emissivity on radiator output. *Energy and Buildings* **2011**, *43*, 400 – 406. doi:https://doi.org/10.1016/j.enbuild.2010.10.002.
16. Munaretto, F.; Recht, T.; Schalbart, P.; Peuportier, B. Empirical validation of different internal superficial heat transfer models on a full-scale passive house. *Journal of Building Performance Simulation* **2017**, *0*, 1–22. doi:10.1080/19401493.2017.1331376.
17. Sevilgen, G.; Kilic, M. Numerical analysis of air flow, heat transfer, moisture transport and thermal comfort in a room heated by two-panel radiators. *Energy and Buildings* **2011**, *43*, 137 – 146. doi:https://doi.org/10.1016/j.enbuild.2010.08.034.
18. Jahanbin, A.; Zanchini, E. Effects of position and temperature-gradient direction on the performance of a thin plane radiator. *Applied Thermal Engineering* **2016**, *105*, 467 – 473. doi:https://doi.org/10.1016/j.applthermaleng.2016.03.018.
19. Maivel, M.; Kurnitski, J. Low temperature radiator heating distribution and emission efficiency in residential buildings. *Energy and Buildings* **2014**, *69*, 224 – 236. doi:https://doi.org/10.1016/j.enbuild.2013.10.030.
20. Maivel, M.; Konzelmann, M.; Kurnitski, J. Energy performance of radiators with parallel and serial connected panels. *Energy and Buildings* **2015**, *86*, 745 – 753. doi:https://doi.org/10.1016/j.enbuild.2014.10.007.
21. ISO 7726:1998. Ergonomics of the thermal environment - Instruments for measuring physical quantities. Standard, International Organization for Standardization, 1998.
22. EQUA. IDA ICE - Indoor Climate and Energy. Technical report, EQUA, Stockholm, Sweden, 2013. http://www.equaonline.com/iceuser/pdf/ice45eng.pdf.
23. ASHRAE. *Standard 55-2004: Thermal environmental conditions for human occupancy Addendum*; Ashrae, 2010.
24. Ferrantelli, A.; Ahmed, K.; Pylsy, P.; Kurnitski, J. Analytical modelling and prediction formulas for domestic hot water consumption in residential Finnish apartments. *Energy and Buildings* **2017**, *143*, 53 – 60. doi:https://doi.org/10.1016/j.enbuild.2017.03.021.
25. EN 442-2:1996/A2:2003. Radiators and Convectors—Part 2: Test Methods and Rating. Technical report, CEN, Bruxelles, BE, 2003.
26. Bring, A.; Sahlin, P.; Vuolle, M. Models for Building Indoor Climate and Energy Simulation. *Journal of Research and Development* **1999**, *21*, 350–359. https://www.equa.se/dncenter/T22Brep.pdf.
27. BS EN 15377-1. Heating systems in buildings - Design of embedded water based surface heating and cooling systems Part 1: Determination of the design heating and cooling capacity. Standard, BSI, 2008.
28. Equa Simulation AB. Validation of IDA Indoor Climate and Energy 4.0 with respect to CEN Standards EN 15255-2007 and EN 15265-2007. Technical report, Equa Simulation AB, Solna, Sweden, 2010.
29. Equa Simulation AB. Validation of IDA Indoor Climate and Energy 4.0 build 4 with respect to ANSI/ASHRAE Standard 140-2004. Technical report, Equa Simulation AB, Solna, Sweden, 2010.
30. Sven Kropf, G.Z. Validation of the Building Simulation Program IDA-ICE According to CEN 13791 "Thermal Performance of Buildings - Calculation of Internal Temperatures of a Room in Summer Without Mechanical Cooling - General Criteria and Validation Procedures". Technical report, Lucerne University of Applied Sciences and Arts, 2013.
31. Peter Loutzenhiser, Heinrich Manz, G.M. Empirical validations of shading/daylighting/load interactions in building energy simulation tools. A report for the International Energy Agency's SHC Task 34/ ECBCS Annex 43 Project C. Technical report, Swiss Federal Laboratories for Material Testing and Research, Iowa State University, 2007.
32. Moosberger, S. IDA ICE CIBSE-Validation: Test of IDA Indoor Climate and Energy version 4.0 according to CIBSE TM33, issue 3. Technical report, HTA Luzern, 2007.
33. Maivel, M.; Kurnitski, J. Radiator and floor heating operative temperature and temperature variation corrections for EN 15316-2 heat emission standard. *Energy and Buildings* **2015**, *99*, 204 – 213. doi:https://doi.org/10.1016/j.enbuild.2015.04.021.

 doi:10.20944/preprints201809.0142.v2

34. Fanger, P. Calculation of thermal comfort-introduction of a basic comfort equation. *ASHRAE Transacions* **1967**, *73*.
35. Olesen, B.W. Thermal comfort. *B & K Technical Review* **1982**, *2*, 3–37.
36. ISO 7730:2005. Ergonomics of the Thermal Environment: Analytical Determination and Interpretation of Thermal Comfort Using Calculation of the PMV and PPD Indices and Local Thermal Comfort Criteria. Standard, International Organization for Standardization, 2005.
37. Hsu, P.C.; Liu, C.; Song, A.Y.; Zhang, Z.; Peng, Y.; Xie, J.; Liu, K.; Wu, C.L.; Catrysse, P.B.; Cai, L.; others. A dual-mode textile for human body radiative heating and cooling. *Science advances* **2017**, *3*, e1700895.

Preprints (www.preprints.org) | NOT PEER-REVIEWED | Posted: 6 November 2018 doi:10.20944/preprints201809.0142.v2

Table A1. Operative temperature t_{op}(°C) in function of panel width and height, 10-type.

Height (m)	0.30	$-0.0046w^2 + 0.0357w + 19.833$
	0.45	$-0.0066w^2 + 0.0494w + 19.839$
	0.60	$-0.0069w^2 + 0.053w + 19.851$
	0.90	$-0.0111w^2 + 0.0786w + 19.859$
Width (m)	0.60	-
	0.80	-
	1.20	$0.1079h + 19.84$
	1.60	$0.1268h + 19.842$
	2.00	$0.1404h + 19.846$
	2.60	$0.1489h + 19.853$
	3.00	$0.1403h + 19.86$

Table A2. Operative temperature t_{op}(°C) in function of panel width and height, 21-type.

Height (m)	0.30	$-0.0031w^2 + 0.0216w + 19.766$
	0.45	$-0.0049w^2 + 0.0355w + 19.773$
	0.60	$-0.0054w^2 + 0.042w + 19.778$
	0.90	$-0.007w^2 + 0.0573w + 19.788$
Width (m)	0.60	$0.0593h + 19.765$
	0.80	$0.0773h + 19.761$
	1.20	$0.0938h + 19.763$
	1.60	$0.1101h + 19.764$
	2.00	$0.125h + 19.764$
	2.60	$0.1408h + 19.764$
	3.00	$0.1509h + 19.763$

Table A3. Formulas for the coefficients in (8) and (9), 10-type.

$\mathbf{A(h)}$	$-0.1074h^3 + 0.1828h^2 - 0.1045h + 0.0132$
$\mathbf{B(h)}$	$0.6012h^3 - 1.0361h^2 + 0.6114h - 0.0707$
$\mathbf{C(h)}$	19.846
$\mathbf{A(w)}$	$-0.0234w^2 + 0.1174w + 3 \times 10^{-5}$
$\mathbf{B(w)}$	$0.0039w^2 - 0.0054w + 19.841$

Table A4. Formulas for the coefficients in (8) and (9), 21-type.

$\mathbf{A(h)}$	$-0.0061h - 0.0017$
$\mathbf{B(h)}$	$0.3025h^3 - 0.5728h^2 + 0.3929h - 0.0529$
$\mathbf{C(h)}$	$0.0741h^3 - 0.1444h^2 + 0.1233h + 19.74$
$\mathbf{A(w)}$	$-0.0084w^2 + 0.0667w + 0.0254$
$\mathbf{B(w)}$	19.763